# Generic Optical Excitations of Correlated Systems: $\pi$-tons

A. Kauch,[1,*] P. Pudleiner,[1,2,*] K. Astleithner,[1] P. Thunström,[3] T. Ribic,[1] and K. Held[1]
[1]Institute of Solid State Physics, TU Wien, 1040 Vienna, Austria
[2]Institute of Theoretical and Computational Physics, Graz University of Technology, 8010 Graz, Austria
[3]Department of Physics and Astronomy, Materials Theory, Uppsala University, 751 20 Uppsala, Sweden

(Received 16 February 2019; revised manuscript received 12 October 2019; published 31 January 2020; corrected 4 March 2020)

The interaction of light with solids gives rise to new bosonic quasiparticles, with the exciton being—undoubtedly—the most famous of these polaritons. While excitons are the generic polaritons of semiconductors, we show that for strongly correlated systems another polariton is prevalent—originating from the dominant antiferromagnetic or charge density wave fluctuations in these systems. As these are usually associated with a wave vector $(\pi, \pi, \ldots)$ or close to it, we propose to call the derived polaritons $\pi$-tons. These $\pi$-tons yield the leading vertex correction to the optical conductivity in all correlated models studied: the Hubbard, the extended Hubbard model, the Falicov-Kimball, and the Pariser-Parr-Pople model, both in the insulating and in the metallic phase.

DOI: 10.1103/PhysRevLett.124.047401

Since the springtime of modern physics, the interaction of solids with light has been of prime interest. The arguably simplest kind of interaction is Einstein's Nobel Prize–winning photoelectric effect [1], where the photon excites an electron across the band gap. More involved processes beyond a mere electron-hole excitation can be described in general by effective bosonic quasiparticles, coined polaritons since a polar excitation is needed to couple the solid to light.

The prime example of a polariton is the exciton [2,3], where the excited electron-hole pair is bound due to the Coulomb attraction between electron and hole. This interaction is visualized in Fig. 1(a). Since it is an attractive interaction, an exciton requires the exciton binding energy less than an unbound electron-hole pair. Other polaritons describe the coupling of the photon to surface plasmons, magnons, or phonons.

Figure 1(b) describes the exciton in terms of Feynman diagrams: the incoming photon creates the electron-hole pair (distinguishable by the different [time] direction of the arrows) which interact with each other repeatedly and finally recombine emitting a photon. Since the energy-momentum relation of light is very steep compared to the electronic band structure of a solid, the transferred momentum from the photon is negligibly small $\mathbf{q} = 0$. Thus, the electron and hole have the same momentum. For semiconductors this is often the preferable momentum transfer as well, connecting the bottom of the conductance with the top of the valence band as in Fig. 1(a).

In this Letter, we show that the generic polaritons for strongly correlated systems are strikingly different. While semiconductors are band insulators with a filled valence and empty conduction band, strongly correlated systems are typically closer to a half-filled (or in general integer filled) band that is split into two Hubbard bands by strong electronic correlations as visualized in Fig. 1(c) for a Mott insulator. (In case of a metallic system there is an additional quasiparticle band). Both metal and insulator are prone to strong antiferromagnetic (AFM) or charge density wave (CDW) fluctuations with a wave vector close to $\mathbf{q} = (\pi, \pi, \ldots)$ [4,5]. Indeed these fluctuations can be described by the central part of the Feynman diagram Fig. 1(b), where the bare ladder diagrams correspond to the random phase approximation (RPA). However the wave vector $\mathbf{q} = (\pi, \pi, \ldots)$ cannot directly couple to light, which

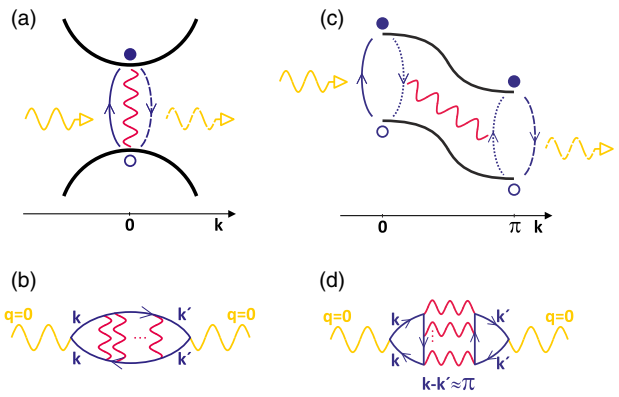


FIG. 1. Sketch of the physical processes (top) and Feynman diagrams (bottom) behind an exciton (left) and a $\pi$-ton (right). The yellow wiggled line symbolizes the incoming (and outgoing) photon, which creates an electron-hole pair denoted by open and filled circles, respectively. The Coulomb interaction between the particles is symbolized by a red wiggled line; dashed line indicates the recombination of the particle and hole; dotted line denotes the creation of a second particle-hole pair (right); black lines the underlying band structure (top panels).

 

only transfers $\mathbf{q} = 0$. Hence an exciton-like polariton as displayed in Fig. 1(b) is not possible for AFM or CDW fluctuations.

As we will show in this Letter, the $(\pi, \pi, \ldots)$ fluctuations nonetheless constitute the dominant vertex corrections beyond a bare (bubble) particle-hole excitation. This is possible through a process where the central part of the Feynman diagram Fig. 1(b), i.e., the $(\pi, \pi, \ldots)$ fluctuations, are rotated (and flipped) as sketched in Fig. 1(d). Now it is possible to transfer $\mathbf{q} = 0$ from the photon and to pick up nonetheless the strong AFM or CDW fluctuations at $\mathbf{k} - \mathbf{k}' \approx (\pi, \pi, \ldots)$. The physics of the associated process is visualized in Fig. 1(c). First, the light creates an electron-hole pair. Through the Coulomb interaction this electron hole-pair creates by impact ionization a second electron-hole pair at a wave vector displaced by $(\pi, \pi, \ldots)$, and the two interact repeatedly with each other, before emitting a photon again. Note that if one assigns times to the electron-photon and Coulomb interactions in Fig. 1(d) there are, after the first and till the last Coulomb interaction, always two particle and two hole Green's functions (cf. the Supplemental Material, Fig. S8 SM). This makes the $\pi$-ton distinctively different from Mott excitons [6–9] or quasiparticle-quasihole excitations, including those envisaged in [10] where the importance of AFM fluctuations was realized.

This excitation resembles to some extent [11] the pairing of electrons in superconductors through magnetic fluctuations. Since AFM or CDW fluctuations are typically at or close to a wave vector $(\pi, \pi, \ldots)$, we suggest to call this polariton a $\pi$-ton. But of course if a strongly correlated system happens to have its dominant fluctuations at another wave vector $\mathbf{k} - \mathbf{k}' \neq 0$, the same processes described in this Letter allow for the coupling to light, creating polaritons.

In hindsight it appears rather obvious that AFM or CDW fluctuations couple this way to light. Why has this not been realized before? This is because numerical methods such as quantum Monte Carlo calculations [10] or exact diagonalization [12] suffer from the difficulty to analyze the underlying physical processes highlighted by the parquet decomposition, and analytical methods such as, e.g., RPA or FLEX [13] have been mostly biased with respect to certain channels such as the particle-hole ($ph$) channel in Fig. 1(b) for excitons. Similar Feynman diagrams but with maximally crossed interaction lines, i.e., the particle-particle ($pp$) channel, have been made responsible for weak localization [14] and strong localization [15] in disordered systems. But the third (rotated) transversal particle-hole ($\overline{ph}$) channel of Fig. 1(d) has, to the best of our knowledge, not been considered hitherto, except for the second-order diagram, the Aslamazov-Larkin correction [16–18], which for half-filling compensates the second-order diagram of the $pp$ channel. Let us emphasize that it is however the whole ladder that is responsible for strong AFM or CDW fluctuations.

Our insight has only been possible because of recent methodological advances that allow us to study all three aforementioned channels unbiasedly, using the parquet equations [19–21] within the dynamical vertex approximation (DΓA) [22–24], the dual fermion approach (DF) [25] and the parquet approximation (PA) [19]. For a review of these and related methods [26–29], see [30].

*Models and methods.*—Let us now turn to the actual calculations, starting with introducing the models, which all can be summarized in the Hamiltonian

$$\mathcal{H} = -t\sum_{\langle ij\rangle\sigma} c^{\dagger}_{i\sigma}c_{j\sigma} + U\sum_{i} n_{i\uparrow}n_{i\downarrow} + \frac{1}{2}\sum_{i\neq j,\sigma\sigma'} V_{ij}n_{i\sigma}n_{j\sigma'}, \quad (1)$$

where $c^{(\dagger)}_{i\sigma}$ represents an annihilation (creation) operator for an electron with spin $\sigma$ at site $i$; $n_{i\sigma} = c^{\dagger}_{i\sigma}c_{i\sigma}$; $\langle ij\rangle$ sums over each nearest neighbor pair $i$, $j$ once. For the Hubbard model (HM) we have a local interaction $U$ only, i.e., $V_{ij} = 0$, and $t$ denotes the hopping. We also study the extended Hubbard model (EHM), with nearest-neighbor interaction $V_{ij} = V$. The Pariser-Parr-Pople model (PPP) [31,32] describes conjugated $\pi$ bonds in carbon-based organic molecules and is here employed for a benzene ring, i.e., a one-dimensional chain with six sites, periodic boundary conditions and interactions between all sites. Finally, the Falicov-Kimball model (FKM) [33,34] has the same form as the HM but the hopping is only for one spin species. All models are solved for the square lattice (except PPP) at half-filling in the paramagnetic phase; $t \equiv 1$ and Planck constant $\hbar \equiv 1$ set our unit of energies and frequencies; for the optical conductivity lattice constant $a \equiv 1$, elementary charge $e \equiv 1$.

We employ the method which we consider most appropriate for the four models, i.e., the parquet DΓA for the HM [35], the PA for the EHM and PPP (which is here more precise than a non-self-consistent DΓA [36,37]), and a parquet variant of the DF, extending earlier DF approaches [38–40]. We solve the parquet equations on a $6 \times 6$ momentum grid, except for the PPP for benzene which has six sites or momenta. For the HM, EHM, and PPP we use the VICTORY code [21] to solve the parquet equations, and W2DYNAMICS [41] to calculate the fully irreducible vertex in case of the HM; for the FKM we employ a reduced frequency structure of the vertex [40,42] implemented in a special-purpose parquet code [43].

The optical conductivity $\sigma(\omega) = \Re\{[\chi^{\mathbf{q}=0}_{jj}(\omega + i\delta) - \chi^{\mathbf{q}=0}_{jj}(i\delta)]/[i(\omega + i\delta)]\}$, for $\delta \to 0$, is calculated from the current-current correlation function $\chi^{\mathbf{q}=0}_{jj}$ at Matsubara frequency $\omega_n$ and momentum $\mathbf{q} = 0$, which can be separated into a bubble term consisting of two Green's functions $G_k$ only and vertex corrections $F^{kk'q}_{d}$ in the following way:

$$\chi_{jj,q} = \frac{2}{\beta N}\sum_{k}[\gamma^{\mathbf{q}}_{\mathbf{k}}]^2 G_{q+k}G_k + \frac{2}{(\beta N)^2}\sum_{k,k'}\gamma^{\mathbf{q}}_{\mathbf{k}}\gamma^{\mathbf{q}}_{\mathbf{k}'}G_{k'}G_{q+k}F_d^{kk'q}G_{q+k'}G_k. \quad (2)$$

Here, we use a four-vector notation $k = (\mathbf{k}, \nu_n)$ with $q = (\mathbf{q} = 0, \omega_n)$; $\gamma^{\mathbf{q}=0}_{\mathbf{k}} = \partial\epsilon_{\mathbf{k}}/\partial\mathbf{k}$ denotes the dipole matrix elements given by the derivative of the energy-momentum relation in the Peierls approximation [44]; $\beta = 1/T$ is the inverse temperature and $N$ the number of $\mathbf{k}$ points.

In the parquet-based approaches employed, the vertex $F$ contains contributions from the fully irreducible vertex $\Lambda$ as well as contributions that are reducible in the three channels ($ph$, $\overline{ph}$, $pp$): $F = \Lambda + \Phi_{ph} + \Phi_{\overline{ph}} + \Phi_{pp}$ [51]. The density component $F_d$ that enters the optical conductivity denotes the even spin combination [20,30].

Inserting in Eq. (2) instead of $F$ one of the summands $\Lambda$, $\Phi_{ph/\overline{ph}/pp}$ we obtain the contributions from the respective channels: $\chi^{\Lambda}$, $\chi^{ph}$, $\chi^{\overline{ph}}$, and $\chi^{pp}$. The most simple contributions to $\chi^{ph}$ and $\chi^{\overline{ph}}$ are just the ladder diagrams of Figs. 1(b) and 1(d), respectively. For the analytic continuation of the optical conductivity to real frequencies we employ the maximum entropy method [53]; for the PPP we use Padé interpolation.

*Results: optical conductivity.*—Let us now turn to the results, starting with the optical conductivity in Fig. 2 (top). Within the four models, we studied five physically different examples: HM (metal), EHM (metal), PPP (insulator), FKM (insulator), and FKM (metal) [see the Supplemental Material [45] for results at different parameters]. In all five cases we see noticeable vertex corrections. For the two insulators, especially for the PPP, there is a strong reduction of the optical gap compared to the one-particle gap (bare bubble contribution $\sigma_0$). Usually one would associate such a reduction to the exciton binding energy. However, when inspecting the contribution of the individual channels in Fig. 2 (bottom), we see that it is not the $ph$ channel of the exciton but the $\overline{ph}$ channel that is dominating and responsible for the reduction of the optical gap. Note that a $ph$ ladder built from a local interaction (RPA) or a local vertex (as, e.g., in dynamical mean field theory [54]) has zero contribution to the optical conductivity [55]. This is why we included in our study also the PPP and EHM where through nonlocal interaction one obtains simple ladder contributions in the $ph$ channel [56].

For two of the metallic cases (HM and FKM) the vertex corrections reduce the conductivity at small frequencies. One might be tempted to associate this with weak localization corrections, i.e., the $pp$ channel. But again by inspecting the vertex contributions in Fig. 2 (bottom) we see that it is the $\overline{ph}$ channel that is dominating; the $pp$ contribution is small. The third metallic case (EHM) is different in the sense that, besides the $\overline{ph}$ channel, the bare vertex $\Lambda$ contributes to a similar amount. This is because the nonlocal interaction provides an additional way to polarize the system and hence to couple to light.

In all cases except for the EHM, the $pp$ channel provides the second largest contribution. One might suspect that this stems from simple RPA-like ladder diagrams as envisaged in the theory of weak localization. But this is not the case. In the case where this $pp$ channel is largest, i.e., for the

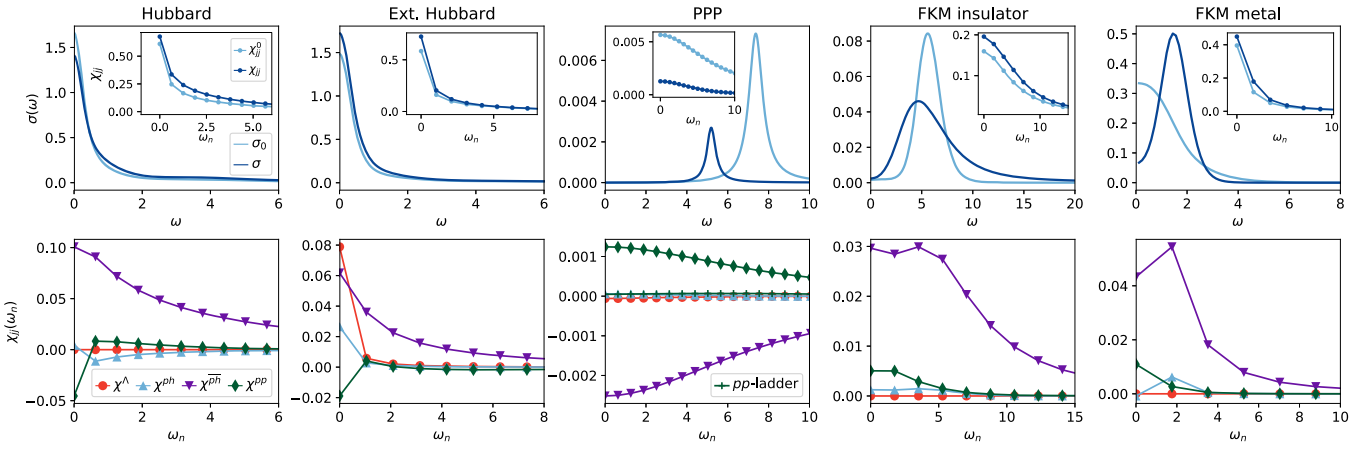


FIG. 2. Top: optical conductivity for real frequency (main panel) and the corresponding current-current correlation function in Matsubara frequencies (insets) of the five cases studied, showing the bare bubble ($\sigma_0$) and the full conductivity ($\sigma$) including vertex corrections (in the insets $\chi^0_{jj}$ and $\chi_{jj}$, respectively). Bottom: corresponding vertex correction to the current-current correlation function $\chi_{jj}$ separated into $ph$, $\overline{ph}$, $pp$, and $\Lambda$ contributions. For the PPP model also the contribution of a RPA-like $pp$ ladder is shown. Parameters from left to right: $U = 4t$, $T = 0.1t$ (HM); $U = 4t$, $T = 0.17t$, $V = t$ (EHM); $T = 0.1t$, $U = 3.962t$, $V_{01} = 2.832t$, $V_{02} = 2.014t$, $V_{03} = 1.803t$ (PPP; interactions translated into units of $t$ are fitted to experiment [57]); $U = 6t$, $T = 0.28t$ (FKM insulator); $U = 2t$, $T = 0.28t$ (FKM metal).

PPP, we additionally plot the contribution from a bare RPA-like $pp$ ladder. It is negligibly small.

*Physical origin of vertex corrections.*—Why does the $\overline{ph}$ channel give such a big contribution? It is because of the dominant fluctuations in the system. These are AFM or CDW fluctuations at a wave vector $(\pi, \pi, \ldots)$ (see below). These fluctuations are already generated by RPA-ladder diagrams in the $ph$ channel and in the $\overline{ph}$ channel as visualized in Fig. 1. Let us emphasize however, that the employed parquet methods take many more Feynman diagrams and the mutual coupling of these channels into account. This coupling, in particular the $pp$ inclusions, leads to a damping of the contribution of the $ph$ and $\overline{ph}$ channels. One can still envisage the physics as in Fig. 1(d) but with a renormalized (screened) interaction and a renormalized propagator.

The fact that, on the other hand, the bare $pp$ ladder in Fig. 2 (bottom middle) is small shows us that there is a strong feedback of the AFM or CDW fluctuations into the $pp$ channel through the parquet equations, which leads to the considerable contributions of the $pp$ channel. In other words, these $pp$ contributions arise (only) as a consequence of the enhanced AFM and CDW fluctuations [58].

To demonstrate the importance of the $(\pi, \pi)$ contribution, we plot in Fig. 3 the reducible contributions $\Phi$ to the full vertex $F$ as a function of $\mathbf{k}' - \mathbf{k}$ for the $ph$ and $\overline{ph}$ channels, setting $\mathbf{q} = 0$ for the optical conductivity. Note that, although the reducible $ph$ and $\overline{ph}$ vertices are interrelated, it is a different momentum and frequency combination that enters the optical conductivity (see the Supplemental Material [45]). As we see in Fig. 3 this $ph$ contribution is small and the $\overline{ph}$ contribution is strongly

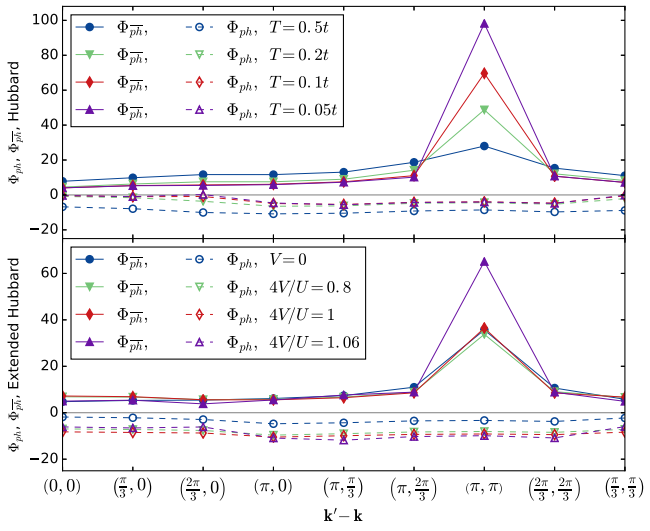


FIG. 3. Reducible contributions $\Phi$ in the $ph$ and $\overline{ph}$ channel to the full vertex $F^{\nu_n \nu'_n \omega_n}_{d,\mathbf{k}\mathbf{k}'\mathbf{q}=0}$ correcting the optical conductivity. Top: HM at various temperatures and $U = 4t$. Bottom: EHM at $U = 4t$, $T = 0.17t$, and various $V$. Shown is the contribution $\nu_n = \nu'_n = \pi T$; $\omega_n = 0$ at fixed $\mathbf{k} = 0$ as a function of $\mathbf{k}' - \mathbf{k}$.

peaked at the wave vector $\mathbf{k}' - \mathbf{k} = (\pi, \pi)$ because of the strong AFM and CDW fluctuations for the HM and EHM, respectively. A similar finding holds for the FKM and PPP model (see the Supplemental Material [45]). Hence we can conclude that it is indeed predominately the $\mathbf{k}' - \mathbf{k} = (\pi, \pi)$ contribution that is responsible for the vertex corrections in the optical conductivity, and therefore we call these polaritons $\pi$-tons.

*Characteristics of the $\pi$-ton.*—While AFM and CDW fluctuations are dominant at all parameters and temperatures analyzed, they become—as a matter of course—stronger when we approach a corresponding phase transition. This effect can be seen in Fig. 3. For the HM (top panel of Fig. 3), reducing the temperature means that AFM fluctuations become strongly enhanced, cf. [24,38,59–61]. While there is no finite-temperature phase transition in two dimensions, the correlation length becomes exponentially large [62]. For the EHM, Fig. 3 (bottom), we instead enhance the nonlocal interaction $V$. This way we approach a phase transition towards CDW ordering (at $4V = U$ in the atomic limit and at a slightly larger $V$s here [37]).

*Conclusion and outlook.*—We have provided compelling evidence for what appears to be the generic polaritons in strongly correlated electron systems—at least in one and two dimensions. These polaritons, coined $\pi$-tons, consist of two particle-hole pairs coupled to the incoming and outgoing light, respectively, and glued together by AFM and CDW fluctuations. Let us emphasize that having two particle-hole pairs (or two holons and two doublons) is a distinct difference to (Mott) excitons [6–9].

In other numerical calculations, $\pi$-tons can be identified by doing a channel diagnostics (see the Supplemental Material [45]). In case of $\pi$-tons it will show the predominance of the particle-hole transversal channel and in case of (Mott) excitons of the particle-hole channel instead. This diagnostics requires only full knowledge of the one- and two-particle Green's functions.

The experimental validation of $\pi$-tons is more challenging. Indeed, the optical conductivity has been studied for a wide range of materials [63–70]. But now that we know that there are $\pi$-tons, too, we need to distinguish these $\pi$-tons from excitons or in metals from weak localization corrections. We see three routes to do so (see the Supplemental Material [45] for an extended discussion). (1) Employing the characteristics of $\pi$-tons to rely on AFM or CDW fluctuations [71], we can employ a control parameter such as temperature, uniaxial pressure or a magnetic field to change these fluctuations. If there are $\pi$-tons there will be corresponding changes in the optical spectrum. Indeed such a characteristic change, specifically an unusual reduction of the optical gap around the Néel temperature, has been already observed in $SmTiO_3$ [67]. To ensure that this effect actually originates from $\pi$-tons excluding a simple reduction of the one-particle gap or spin-polaron formations [6,7,72–74], additional angular

resolved photoemission spectroscopy (ARPES) and inverse ARPES are necessary as a function of the control parameter. (2) In a joint experimental and theoretical effort we can take the experimental one-particle spectrum $A_{\mathbf{k}\nu}$ (as, e.g., measured in ARPES and inverse ARPES) and the experimental dynamic spin susceptibility $\chi_m(\mathbf{q},\omega)$ (as, e.g., measured by neutron spectroscopy) and calculate from this the optical conductivity $\sigma(\omega)$ including $\pi$-tons and compare it with the measured one. (3) Last but not least we can do *ab initio* calculations of strongly correlated materials for which $\pi$-tons may be expected, e.g., along the line of [75], and calculate the optical spectrum including $\pi$-tons and exciton contributions. Given good agreement with experiment and sizable $\pi$-ton effects, this would provide excellent evidence for $\pi$-tons.

We would like to thank Jan Kuneš, Gang Li, Angelo Valli, and Paul Worm for many stimulating discussions, Josef Kaufmann and Clemens Watzenböck for the help with analytic continuation, and Monika Waas for graphical assistance. The present work was supported by the European Research Council under the European Union's Seventh Framework Program (FP/2007-2013) through ERC Grant No. 306447, the Austrian Science Fund (FWF) through Project No. P 30997-N32 and Doctoral School "Building Solids for Function" (P. P.). Calculations have been done on the Vienna Scientific Cluster (VSC).

*These authors contributed equally to this work.

[1] A. Einstein, Ann. Phys. (Berlin) **322**, 132 (1905).
[2] J. Frenkel, Phys. Rev. **37**, 17 (1931).
[3] G. H. Wannier, Phys. Rev. **52**, 191 (1937).
[4] B. Keimer, Recent advances in experimental research on high-temperature superconductivity, in *Autumn School on Correlated Electrons Emergent Phenomena in Correlated Matter*, edited by E. Pavarini, E. Koch, and U. Schollwöck (Forschungszentrum Jülich, Jülich, 2013.
[5] G. Aeppli, J. Magn. Magn. Mater. **272–276**, 7 (2004).
[6] D. G. Clarke, Phys. Rev. B **48**, 7520 (1993).
[7] P. Wróbel and R. Eder, Phys. Rev. B **66**, 035111 (2002).
[8] F. H. L. Essler, F. Gebhard, and E. Jeckelmann, Phys. Rev. B **64**, 125119 (2001).
[9] E. Jeckelmann, Phys. Rev. B **67**, 075106 (2003).
[10] N. Lin, E. Gull, and A. J. Millis, Phys. Rev. B **80**, 161105 (R) (2009).
[11] Different is that in a superconductor two particles interact through repeated ladders, here two electron-hole pairs interact through a single ladder.
[12] J. Vučičević, J. Kokalj, R. Žitko, N. Wentzell, D. Tanasković, and J. Mravlje, Phys. Rev. Lett. **123**, 036601 (2019).
[13] H. Kontani, J. Phys. Soc. Jpn. **75**, 013703 (2006).
[14] B. L. Altshuler and A. G. Aronov, Electron-electron interaction in disordered conductors, in *Electron-Electron Interaction in Disordered Conductors*, edited by A. I. Efros and M. Pollak (Elsevier Science Publisher, North Holland, 1985).
[15] E. Abrahams, P. W. Anderson, D. C. Licciardello, and T. V. Ramakrishnan, Phys. Rev. Lett. **42**, 673 (1979).
[16] L. G. Aslamazov and A. I. Larkin, Sov. Phys. Solid State **10**, 875 (1968).
[17] D. Bergeron, V. Hankevych, B. Kyung, and A.-M. S. Tremblay, Phys. Rev. B **84**, 085128 (2011).
[18] A. V. Chubukov, D. L. Maslov, and V. I. Yudson, Phys. Rev. B **89**, 155126 (2014).
[19] N. E. Bickers, *Theoretical Methods for Strongly Correlated Electrons* (Springer-Verlag, New York, Berlin Heidelberg, 2004), pp. 237–296.
[20] G. Li, N. Wentzell, P. Pudleiner, P. Thunström, and K. Held, Phys. Rev. B **93**, 165103 (2016).
[21] G. Li, A. Kauch, P. Pudleiner, and K. Held, Comput. Phys. Commun. **241**, 146 (2019).
[22] A. Toschi, A. A. Katanin, and K. Held, Phys. Rev. B **75**, 045118 (2007).
[23] H. Kusunose, J. Phys. Soc. Jpn. **75**, 054713 (2006).
[24] A. A. Katanin, A. Toschi, and K. Held, Phys. Rev. B **80**, 075104 (2009).
[25] A. N. Rubtsov, M. I. Katsnelson, and A. I. Lichtenstein, Phys. Rev. B **77**, 033101 (2008).
[26] G. Rohringer, A. Toschi, H. Hafermann, K. Held, V. I. Anisimov, and A. A. Katanin, Phys. Rev. B **88**, 115112 (2013).
[27] C. Taranto, S. Andergassen, J. Bauer, K. Held, A. Katanin, W. Metzner, G. Rohringer, and A. Toschi, Phys. Rev. Lett. **112**, 196402 (2014).
[28] T. Ayral and O. Parcollet, Phys. Rev. B **92**, 115109 (2015).
[29] G. Li, Phys. Rev. B **91**, 165134 (2015).
[30] G. Rohringer, H. Hafermann, A. Toschi, A. A. Katanin, A. E. Antipov, M. I. Katsnelson, A. I. Lichtenstein, A. N. Rubtsov, and K. Held, Rev. Mod. Phys. **90**, 025003 (2018).
[31] J. A. Pople, Trans. Faraday Soc. **49**, 1375 (1953).
[32] R. Pariser and R. G. Parr, J. Chem. Phys. **21**, 466 (1953).
[33] L. M. Falicov and J. C. Kimball, Phys. Rev. Lett. **22**, 997 (1969).
[34] J. K. Freericks and V. Zlatić, Rev. Mod. Phys. **75**, 1333 (2003).
[35] A. Kauch, F. Hörbinger, G. Li, and K. Held, arXiv:1901.09743.
[36] P. Pudleiner, P. Thunström, A. Valli, A. Kauch, G. Li, and K. Held, Phys. Rev. B **99**, 125111 (2019).
[37] P. Pudleiner, A. Kauch, K. Held, and G. Li, Phys. Rev. B **100**, 075108 (2019).
[38] J. Otsuki, H. Hafermann, and A. I. Lichtenstein, Phys. Rev. B **90**, 235132 (2014).
[39] S.-X. Yang, P. Haase, H. Terletska, Z. Y. Meng, T. Pruschke, J. Moreno, and M. Jarrell, Phys. Rev. B **89**, 195116 (2014).
[40] T. Ribic, G. Rohringer, and K. Held, Phys. Rev. B **93**, 195105 (2016).
[41] M. Wallerberger, A. Hausoel, P. Gunacker, A. Kowalski, N. Parragh, F. Goth, K. Held, and G. Sangiovanni, Comput. Phys. Commun. **235**, 388 (2019).
[42] T. Ribic, G. Rohringer, and K. Held, Phys. Rev. B **95**, 155130 (2017).
[43] K. Astleithner, A. Kauch, T. Ribic, and K. Held, arXiv:1912.01908.

[44] Except for the PPP model where $\gamma_{\mathbf{k}} \equiv 1$, which corresponds to the dynamical compressibility; for additional results with $\gamma_{\mathbf{k}}^{\mathbf{q}=0} = \partial\epsilon_{\mathbf{k}}/\partial\mathbf{k}$ see the Supplemental Material [45].
[45] See Supplemental Material at http://link.aps.org/supplemental/10.1103/PhysRevLett.124.047401 for an extended discussion, which includes Refs. [45–49].
[46] E. Pavarini, A. Yamasaki, J. Nuss, and O. K. Andersen, New J. Phys. **7**, 188 (2005).
[47] T. A. Maier, M. Jarrell, and D. J. Scalapino, Phys. Rev. B **75**, 134519 (2007).
[48] A. T. Rømer, A. Kreisel, I. Eremin, M. A. Malakhov, T. A. Maier, P. J. Hirschfeld, and B. M. Andersen, Phys. Rev. B **92**, 104505 (2015).
[49] A. P. Kampf and W. Brenig, Z. Phys. B **89**, 313 (1992).
[50] L. Si, Z. Zhong, J. M. Tomczak, and K. Held, Phys. Rev. B **92**, 041108(R) (2015).
[51] For a similar analysis for the self-energy, cf. [52].
[52] O. Gunnarsson, T. Schäfer, J. P. F. LeBlanc, J. Merino, G. Sangiovanni, G. Rohringer, and A. Toschi, Phys. Rev. B **93**, 245102 (2016).
[53] D. Geffroy, J. Kaufmann, A. Hariki, P. Gunacker, A. Hausoel, and J. Kuneš, Phys. Rev. Lett. **122**, 127601 (2019).
[54] A. Georges, G. Kotliar, W. Krauth, and M. J. Rozenberg, Rev. Mod. Phys. **68**, 13 (1996).
[55] Because $G_{q+k}G_k$ in Eq. (2) is even in $\mathbf{k}$ for $\mathbf{q} = 0$ and $\gamma_{\mathbf{k}}^{\mathbf{q}=0}$ is odd.
[56] The nonzero $ph$ contributions in the HM and FKM stem from insertions of other diagrams into the $ph$ ladder through the parquet equations.
[57] R. J. Bursill, C. Castleton, and W. Barford, Chem. Phys. Lett. **294**, 305 (1998).
[58] In contrast, the bare $ph$ ladder would be much larger without feedback from the other channels.
[59] G. Rohringer, A. Toschi, A. Katanin, and K. Held, Phys. Rev. Lett. **107**, 256402 (2011).
[60] T. Schäfer, A. A. Katanin, K. Held, and A. Toschi, Phys. Rev. Lett. **119**, 046402 (2017).
[61] J. Gukelberger, E. Kozik, and H. Hafermann, Phys. Rev. B **96**, 035152 (2017).
[62] T. Schäfer, F. Geles, D. Rost, G. Rohringer, E. Arrigoni, K. Held, N. Blümer, M. Aichhorn, and A. Toschi, Phys. Rev. B **91**, 125109 (2015).
[63] D. N. Basov, R. D. Averitt, D. van der Marel, M. Dressel, and K. Haule, Rev. Mod. Phys. **83**, 471 (2011).
[64] S. Uchida, T. Ido, H. Takagi, T. Arima, Y. Tokura, and S. Tajima, Phys. Rev. B **43**, 7942 (1991).
[65] S. Tajima, Rep. Prog. Phys. **79**, 094001 (2016).
[66] P. Lunkenheimer, F. Mayr, and A. Loidl, Ann. Phys. (Berlin) **15**, 498 (2006).
[67] A. Gössling, R. Schmitz, H. Roth, M. W. Haverkort, T. Lorenz, J. A. Mydosh, E. Müller-Hartmann, and M. Grüninger, Phys. Rev. B **78**, 075122 (2008).
[68] A. Gössling, M. W. Haverkort, M. Benomar, H. Wu, D. Senff, T. Möller, M. Braden, J. A. Mydosh, and M. Grüninger, Phys. Rev. B **77**, 035109 (2008).
[69] I. Lo Vecchio, L. Baldassarre, F. D'Apuzzo, O. Limaj, D. Nicoletti, A. Perucchi, L. Fan, P. Metcalf, M. Marsi, and S. Lupi, Phys. Rev. B **91**, 155133 (2015).
[70] J. Ruppen, J. Teyssier, I. Ardizzone, O. E. Peil, S. Catalano, M. Gibert, J.-M. Triscone, A. Georges, and D. van der Marel, Phys. Rev. B **96**, 045120 (2017).
[71] Possibly also orbital fluctuations with $\mathbf{q} = (\pi, \pi, \ldots)$.
[72] G. Martinez and P. Horsch, Phys. Rev. B **44**, 317 (1991).
[73] G. Sangiovanni, A. Toschi, E. Koch, K. Held, M. Capone, C. Castellani, O. Gunnarsson, S.-K. Mo, J. W. Allen, H.-D. Kim, A. Sekiyama, A. Yamasaki, S. Suga, and P. Metcalf, Phys. Rev. B **73**, 205121 (2006).
[74] C. Taranto, G. Sangiovanni, K. Held, M. Capone, A. Georges, and A. Toschi, Phys. Rev. B **85**, 085124 (2012).
[75] A. Galler, P. Thunström, P. Gunacker, J. M. Tomczak, and K. Held, Phys. Rev. B **95**, 115107 (2017).

*Correction:* In the front matter, equal-contributor indicators were incorrectly ascribed; these indicators have now been assigned properly.